HeerscheJarillo-HerreroOostingaVandersypenMorpurgo2007

Available online at www.sciencedirect.com

ScienceDirect

Solid State Communications 143 (2007) 72–76

solid state communications

www.elsevier.com/locate/ssc

Induced superconductivity in graphene

Hubert B. Heersche, Pablo Jarillo-Herrero[1], Jeroen B. Oostinga, Lieven M.K. Vandersypen, Alberto F. Morpurgo*

Kavli Institute of Nanoscience, Delft University of Technology, PO Box 5046, 2600 GA, Delft, The Netherlands

Accepted 19 February 2007 by A. Geim
Available online 27 April 2007

Abstract

Graphene layers, prepared by mechanical exfoliation, were contacted by superconducting electrodes consisting of a titanium–aluminium bilayer. Quantum hall measurements in the normal state confirmed the single layer nature of the graphene samples. Proximity induced supercurrents were observed in all samples, below 1 K. Using a backgate, the Fermi energy could be swept from valence to conduction band via the Charge neutrality point, demonstrating supercurrents carried by holes and electrons, respectively. Interestingly, a finite supercurrent was also observed at the charge neutrality (or Dirac) point, where the density of carrier states vanishes. Our results demonstrate phase coherence in graphene.

PACS: 73.63.-b; 74.50.+r; 81.05.Uw

Keywords: A. Graphene; D. Josephson effect; D. Superconductivity

1. Introduction

Recent transport measurements performed on graphene – a one-atom-thick layer of graphite – have led to a series of surprising observations. Phenomena such as the integer quantum Hall effect [1,2] and weak-localization [3,4], for instance, do not conform to the well-established theory of electronic transport in two-dimensional systems. As the theory has been developed to describe the behaviour of two-dimensional electron gases hosted in conventional semiconducting heterostructures, for which it works quantitatively with impressive accuracy, the unexpected behaviour observed in graphene suggests that this material is fundamentally different. Indeed, it is now understood that the anomalous behaviour of graphene originates from the fact that, at low energy, the dynamics of electrons is governed by the relativistic Dirac equation for massless particles, rather than the conventional Schrödinger equation [5,6]. Although more than twenty years ago it was already appreciated that graphene could represent an experimental realization of a system of relativistic Dirac fermions [7], this fact was considered as having mere academic value until last year. Now, with the first transport experiments through graphene having been performed successfully [1,2], it is becoming more and more clear that graphene does not only have academic value, but that this material does establish a new paradigm in condensed matter physics.

The microscopic properties of Dirac electrons are very different from those of electrons described by the Schrödinger equation. For instance, the wave-function of Dirac electrons in graphene has two components due to the presence of two independent atoms in the unit cell of the material. This results in the so-called pseudo-spin. An additional quantum number is also present, which determines to which of the two independent valleys of graphene (the K and K' valley) the quantum state of electrons in graphene belong. Other important differences are the linear dispersion relation and the absence of a gap between conduction and valence band (graphene is a zero-gap semiconductor). Owing to these differences, it is expected that many transport phenomena that have been studied, and are well-understood, in conventional 2DEGs will exhibit an anomalous

* Corresponding author.
E-mail addresses: J.B.Oostinga@tudelft.nl (J.B. Oostinga), a.morpurgo@tnw.tudelft.nl (A.F. Morpurgo).
[1] Present address: Columbia Physics Department, 538 West 120th Street, Mail code 9330, New York, NY 10027, USA.

0038-1098/$ - see front matter © 2007 Elsevier Ltd. All rights reserved.
doi:10.1016/j.ssc.2007.02.044

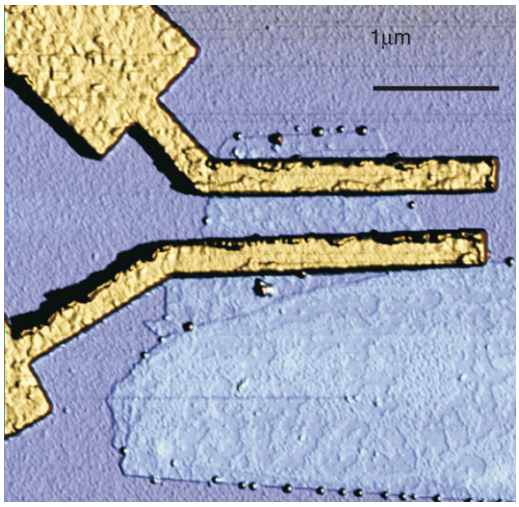

Fig. 1. An atomic force microscopy image of a single layer graphene sheet with two superconducting electrodes.

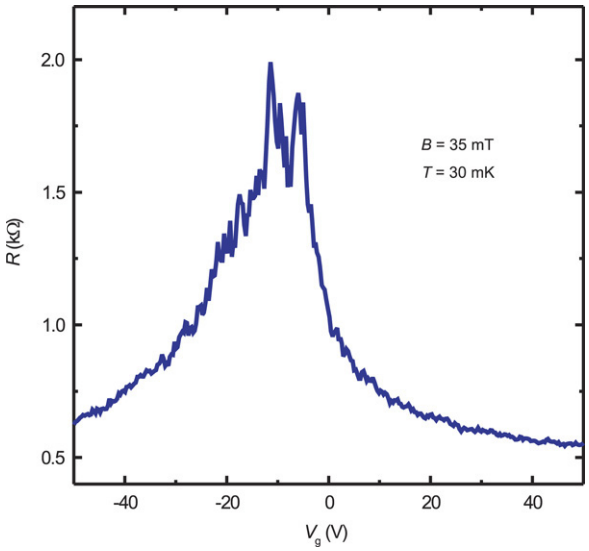

Fig. 2. Two terminal resistance measurement as function of the gate voltage showing the finite resistance at the charge neutrality point. A small magnetic field is applied to drive the electrodes into the normal state.

behaviour in graphene. The integer quantum Hall effect and weak localization are only the first examples and it is important to investigate a much broader variety of phenomena.

Here, we report a systematic investigation of induced superconductivity through graphene layers contacted with superconducting electrodes (first published in Ref. [8]). From a technical point of view graphene is particularly suitable for these experiments because low-resistance electrical contact can be prepared fairly easily, by simply evaporating metals onto the surface of the material. Of particular interest is the possibility to use a gate voltage to tune the carrier concentration, so that the Fermi level can be swept from the conduction to the valence band. This permits investigation of the occurrence of proximity effect mediated by either electrons or holes in graphene, and to study behaviour near the charge neutrality point. Our experiments demonstrate the occurrence of induced superconductivity in graphene in all its basic manifestations.

2. Sample fabrication and characterization

The work described here relies on Josephson junctions realized on graphene layers contacted by two closely spaced superconductors. Single and few layer graphene junctions are fabricated on oxidized Si substrates by mechanical exfoliation of bulk graphite [9], followed by optical microscope inspection to locate the thinnest graphitic flakes, and electron beam lithography to define electrical contacts. Fig. 1 shows an atomic force microscopy (AFM) image of a typical device. We use as superconducting contacts a Ti/Al bilayer (10/70 nm). Titanium ensures good electrical contact to graphene and Al establishes a sufficiently high critical temperature to enable the observation of a supercurrent in a dilution refrigeration set-up [10]. Before discussing their superconducting properties, we first characterize the devices with the superconducting electrodes in the normal state. Fig. 2 shows the two-terminal resistance, R, versus gate voltage, V_G, for one of our samples. The strong V_G-dependence of R provides a first indication that the device consists of at most a few layers of graphene [9], since, due to screening, V_G affects the carrier density only in the bottom one or two layers. For single layers, the position of the resistance maximum corresponds to the gate voltage at which the Fermi energy is located at the charge neutrality point, V_D, and we typically find that $|V_D| < 20$ V. We unambiguously determine the single layer character of a device by quantum Hall effect (QHE) measurements. Because the superconducting proximity effect requires two closely spaced electrodes, we can only perform magnetoconductance measurements in a two terminal configuration. In general, the conductance, G, measured in this way is a mixture of longitudinal and Hall signals, but at high fields $G \approx |G_{\mathrm{Hall}}|$ (this approximation is exact at the Hall plateaus [11]). Indeed, the measurement of G versus V_G at $B = 10$ T shows clearly identifiable Hall plateaus at half-integer multiples of $4e^2/h$ (Fig. 3), characteristic of the QHE in single layer graphene [1,2]. This demonstrates that, even in mesoscopic samples, the quantum Hall effect can be used to identify single layer devices. (The data shown are representative of the general behaviour observed; All the measurements shown have been taken on the same device, except Figs. 5 and 6, which correspond to different single layer devices).

3. Experimental manifestations of induced superconductivity

Cooling down the devices below the critical temperature of the electrodes ($T_c \sim 1.3$ K) leads to proximity-induced superconductivity in the graphene layer. A direct proof of induced superconductivity is the observation of a Josephson supercurrent [12]. Fig. 4 shows the current–voltage (I–V) characteristics of a single layer device. The current flows without resistance (no voltage drop at finite current) below the critical current, I_c (what we actually measure is the switching current; the intrinsic I_c may be higher [12,13]). In our devices, I_c ranged from ~10 nA to more than 800 nA, depending of the width of the graphene layer, the separation of the contacts and

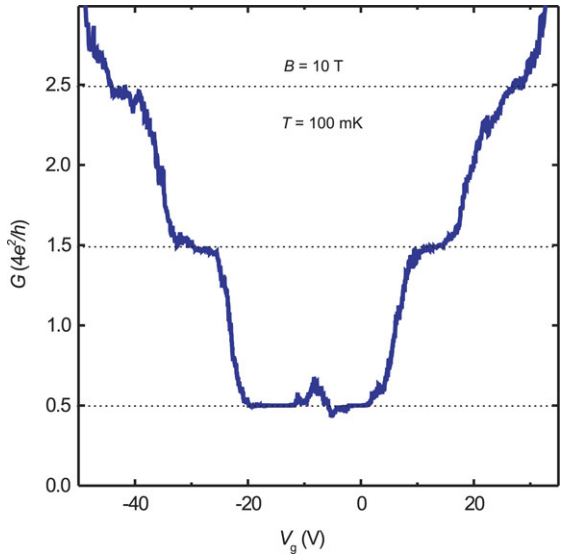

Fig. 3. Two terminal conductance measurement as function of the gate voltage at high magnetic field showing plateaus at $2e^2/h$, $6e^2/h$ and $10e^2/h$.

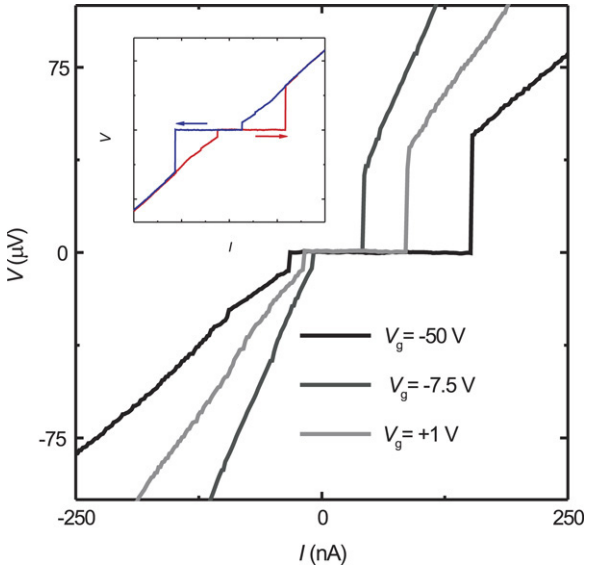

Fig. 4. Voltage measurements as function of current bias measured at different gate voltages showing a gate dependent critical current ($T = 30$ mK). The inset shows current bias sweeps from negative to positive values and vice versa. The retrapping current is smaller than the switching current, as is typical for underdamped Josephson junctions.

the value of the gate voltage. Remarkably, we have measured proximity-induced supercurrents in all the devices that we tested (17 flakes in total, with several devices on some flakes), including four flakes that were unambiguously identified as single-layer graphene via QHE (the rest being probably two to four layers thick). The temperature and magnetic field dependence of the measured critical current are shown in Figs. 5 and 6. The periodicity (2.5 ± 0.5 mT) of the oscillations in the Fraunhofer pattern corresponds well to a flux quantum Φ_o divided by the junction area (0.7 ± 0.2 μm^2). In addition, the many lobes of decreasing amplitude clearly visible in the pattern indicate that the supercurrent density distribution [14] is spatially uniform.

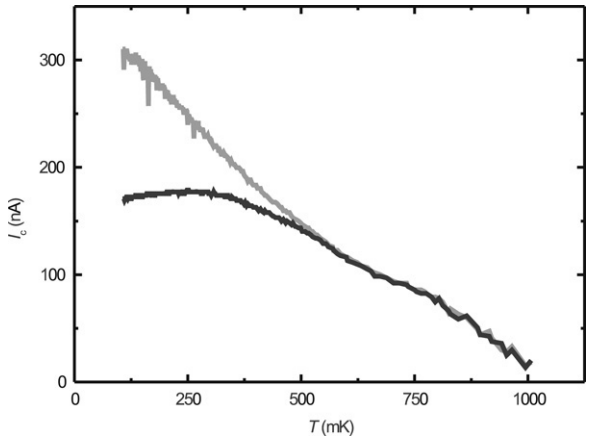

Fig. 5. The temperature dependence of the critical current ($V_g = 0$ V). The black and the grey curves are the retrapping current and the switching current, respectively.

Having established the existence of the Josephson effect in graphene, we analyse the gate voltage dependence of the critical current. Fig. 4 shows several I–V traces taken at different V_G, where it can already be seen that varying the gate voltage has a strong effect on the maximum supercurrent flowing through the device. This behaviour can be more readily seen in Fig. 6, where the differential resistance is plotted as a function of current bias and gate voltage. By changing V_G we can shift continuously the Fermi energy from the valence band ($V_G < V_D$) to the conduction band ($V_G > V_D$): irrespective of the sign of V_G, we find a finite supercurrent. This demonstrates that the devices operate as bipolar supercurrent transistors: the supercurrent is carried by hole Cooper pairs when the Fermi level is in the valence band and by electron Cooper pairs when it is in the conduction band. Note that in going from valence to conduction band, we sweep the position of the Fermi level through the charge neutrality point. Strikingly, even then the supercurrent remains finite, despite the fact that for perfect graphene theory predicts a vanishing density of states at $V_G = V_D$ [15]. This behaviour has been observed in all samples and demonstrates that electronic transport in graphene is phase coherent irrespective of the gate voltage, including when the Fermi level is located at the charge neutrality point.

In conventional Josephson junctions, the critical current correlates with the normal state conductance, G_n [16]. In graphene this correlation can be observed directly, as shown in Fig. 7, because both I_c and G_n depend on V_G. To analyse this correlation, we plot the product of the measured critical current and the normal state resistance ($R_n = 1/G_n$), or I_cR_n product (see Fig. 8). We find that at high gate voltage $I_cR_n \approx \Delta/e$, and that I_cR_n is suppressed by a factor 2-3 around the charge neutrality point. The observed I_cR_n-product is thus close to the theoretical value of $\sim 2.5\Delta/e$ for a model system of graphene in the ballistic regime [17]. The remaining discrepancy may be accounted for by the difference between the measured critical current (or switching current) and the intrinsic critical current [12,13].

The induced superconductivity in graphene manifests itself also at finite bias in the form of subgap structure in the

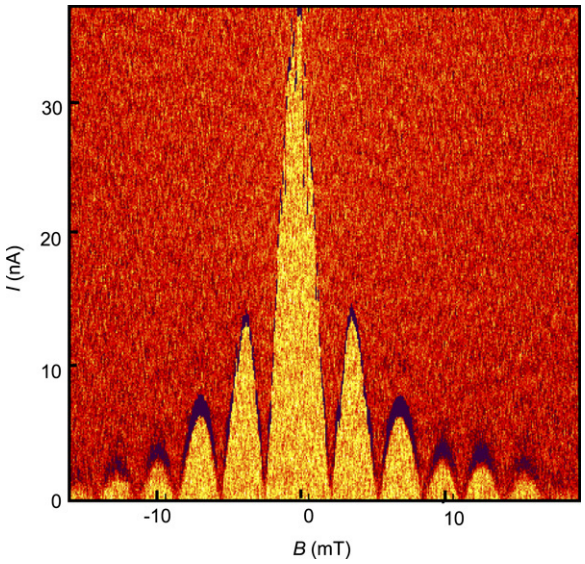

Fig. 6. Colour-scale representation of the differential resistance, $\mathrm{d}V/\mathrm{d}I$, as function of current bias and magnetic field ($T = 30$ mK, $V_g = 0$ V). The light coloured and the dark coloured regions correspond to the supercurrent regime and the normal regime, respectively. The critical current versus magnetic field shows a Fraunhofer-like pattern.

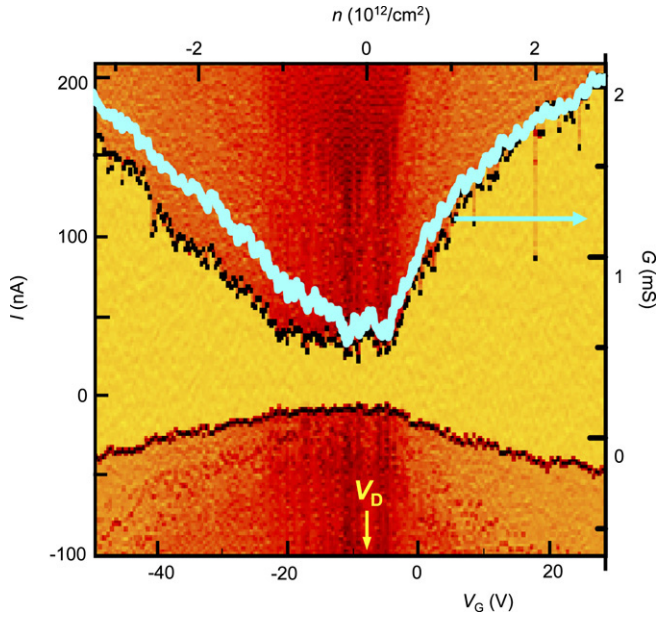

Fig. 7. Colour-scale representation of the differential resistance, $\mathrm{d}V/\mathrm{d}I$, as function of current bias and gate voltage ($T = 30$ mK). The light coloured region is the supercurrent regime and the dark coloured region is the normal regime. The top axis shows the electron density, n, as obtained from geometrical considerations. Note that the critical current is not symmetrical with respect to the charge neutrality point, V_D. The origin of this asymmetry is not known, but similar asymmetry is seen in the normal state conductance (grey curve).

differential resistance due to multiple Andreev reflections [18], as shown in Fig. 9. This subgap structure consists of a series of minima at source-drain voltages $V = 2\Delta/en$ ($n = 1, 2\ldots$), which enables us to determine the superconducting gap. We find $\Delta = 125$ μeV as expected for our Ti/Al bilayers [10]. The position of the minima is essentially independent of the gate voltage. The sharpness of the features associated to multiple

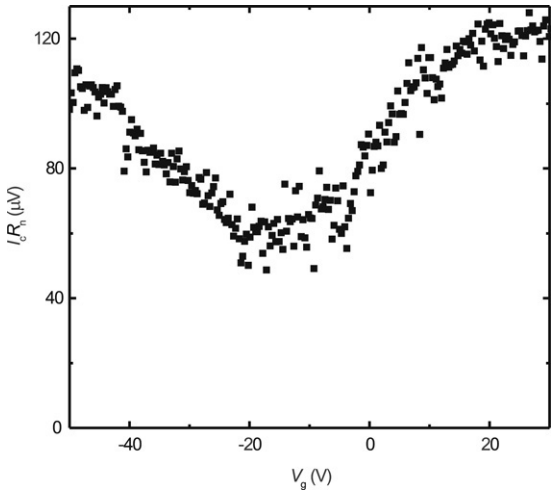

Fig. 8. Product of the critical current and the normal state resistance plotted versus the gate voltage. The normal state resistance is measured at zero source-drain bias, at $T = 30$ mK and with a small magnetic field to drive the electrodes in the normal state.

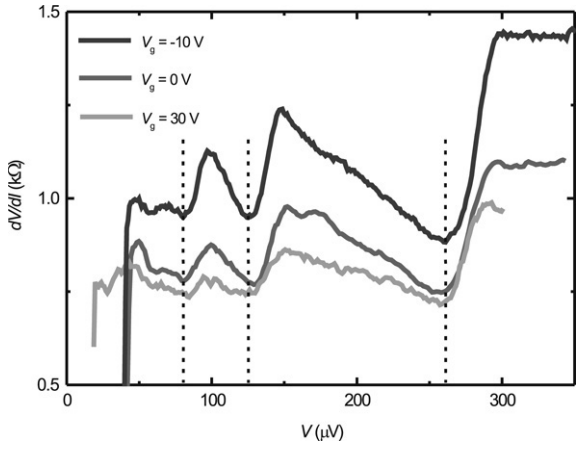

Fig. 9. The differential resistance, $\mathrm{d}V/\mathrm{d}I$, versus the voltage bias measured at different gate voltages (the charge neutrality point is around $V_g = -10$ V). The traces show multiple Andreev reflection dips at voltages below twice the superconducting energy gap ($T = 30$ mK).

Andreev reflection, on the contrary, does depend on gate voltage. Although we have not performed a fully quantitative analysis, it appears that these features are sharper when the gate voltage is close to the charge neutrality point, in qualitative agreement with recent theoretical calculations [19]. In all cases, for $V > 2\Delta/e$, the differential resistance returns to the normal state value. From the suppression in differential resistance observed while changing the bias from above to below the gap, we can estimate that the average transparency of the superconductor–graphene interface is ∼0.7–0.8.

4. Conclusions

The experiments discussed above show that all the main phenomena characteristic of induced superconductivity can be observed in graphene Josephson junctions. It is worth noting that these experiments show that the occurrence of a Josephson supercurrent in graphene is a robust and very reproducible phenomenon. This is not to be expected a

priori, because Josephson supercurrent requires phase coherent transport and the presence of time reversal symmetry and previous measurements of weak localization – that also requires phase coherence and time reversal symmetry to be present – have shown an unexpected irreproducibility (the weak-localization signal is strongly sample dependent and often absent) [3,4]. As discussed elsewhere (see Ref. [8] for details), this difference between weak-localization and Josephson supercurrent originates from the presence of two different K-points, and is therefore a manifestation of the unique electronic properties of graphene.

Acknowledgements

We gratefully acknowledge A. Geim, D. Jiang and K. Novoselov for help with device fabrication; L. Kouwenhoven for the use of experimental equipment, support and discussions; C. Beenakker, J. van Dam, D. Esteve, T. Klapwijk, Y. Nazarov, G. Steele, B. Trauzettel, C. Urbina and B. van Wees for helpful discussions. We thank FOM and NWO for financial support.

References

[1] K.S. Novoselov, A.K. Geim, S.V. Morozov, D. Jiang, M.I. Katsnelson, I.V. Grigorieva, S.V. Dubonos, A.A. Firsov, Nature 438 (2005) 197.
[2] Y.B. Zhang, Y.W. Tan, H.L. Stormer, P. Kim, Nature 438 (2005) 201.
[3] S.V. Morozov, K.S. Novoselov, M.I. Katsnelson, F. Schedin, L.A. Ponomarenko, D. Jiang, A.K. Geim, Physical Review Letters 97 (2006).
[4] A.F. Morpurgo, F. Guinea, Physical Review Letters 97 (2006).
[5] V.P. Gusynin, S.G. Sharapov, Physical Review Letters 95 (2005).
[6] N.M.R. Peres, F. Guinea, A.H.C. Neto, Physical Review B 73 (2006).
[7] G.W. Semenoff, Physical Review Letters 53 (1984) 2449.
[8] H.B. Heersche, P. Jarillo-Herrero, J.B. Oostinga, L.M.K. Vandersypen, A.F. Morpurgo, Nature 446 (2007) 56.
[9] K.S. Novoselov, A.K. Geim, S.V. Morozov, D. Jiang, Y. Zhang, S.V. Dubonos, I.V. Grigorieva, A.A. Firsov, Science 306 (2004) 666.
[10] P. Jarillo-Herrero, J.A. van Dam, L.P. Kouwenhoven, Nature 439 (2006) 953.
[11] S. Datta, Electronic Transport in Mesoscopic Systems, Cambridge University Press, Cambridge, 1995.
[12] M. Tinkham, Introduction to Superconductivity, 2nd ed., McGraw-Hill, Singapore, 1996.
[13] P. Joyez, P. Lafarge, A. Filipe, D. Esteve, M.H. Devoret, Physical Review Letters 72 (1994) 2458.
[14] A. Barone, G. Paterno, Physics and Applications of the Josephson Effect, John Wiley & Sons, New York, 1982.
[15] M.S. Dresselhaus, G. Dresselhaus, P.C. Eklund, Science of Fullerenes and Carbon Nanotubes, Academic Press, San Diego, 1996.
[16] K.K. Likharev, Reviews of Modern Physics 51 (1979) 101.
[17] M. Titov, C.W.J. Beenakker, Physical Review B 74 (2006) 041401(R).
[18] M. Octavio, M. Tinkham, G.E. Blonder, T.M. Klapwijk, Physical Review B 27 (1983) 6739.
[19] J.C. Cuevas, A.L. Yeyati, Physical Review B 74 (2006).